Available online at www.sciencedirect.com
SCIENCE DIRECT
Catalysis Today 113 (2006) 126–130
CATALYSIS TODAY
www.elsevier.com/locate/cattod

Probing the pore space in mesoporous materials by laser enhanced hyperpolarised ^{129}Xe NMR

F. Guenneau, M. Nader, P. Salamé, F. Launay, V. Semmer-Herledan, A. Gédéon *

Laboratoire Systèmes Interfaciaux à l'Echelle Nanométrique, CNRS UMR 7142, Université Pierre et Marie Curie, 4, place Jussieu, 75252 Paris, France

Available online 19 January 2006

Abstract

Laser hyperpolarised (HP) ^{129}Xe NMR technique has been used to study the porous structure of ordered purely siliceous MCM-41, SBA-15 and functionalised mesoporous materials and mesoporous SiO_2 thin films. The use of hyperpolarised xenon allows us to measure spectra at very low concentrations of xenon where xenon reflects mainly interaction between the adsorbed xenon atoms and the surface. Variable temperature measurements allowed us to obtain information on the heat of adsorption of xenon on the surface and to evaluate the chemical shift of xenon interacting with the surface.

Keywords: Xenon; Mesoporous; Hyperpolarised; NMR

1. Introduction

The ^{129}Xe NMR spectroscopy is a powerful technique for the characterisation of porous solids [1,2]. Its main advantage is the high sensitivity of the chemical shift of ^{129}Xe to its local environment. However, the application of thermally polarised ^{129}Xe NMR to materials, viz to mesoporous silica [3], is often hampered by a relatively weak signal-to-noise ratio due to low concentration of adsorbed xenon and long relaxation times. An increase in sensitivity of several orders of magnitude (up to a factor 10^4) can be achieved by using optical pumping techniques to produce hyperpolarised (HP) xenon [4]. Recent advances including HP Xe delivery into MAS probes [5] and circulating continuous flow systems [6] made it very attractive for materials applications [7] and allowed to probe very small quantities of matter [8].

Since 1991, great interest has been drawn to a new class of mesoporous materials, i.e. MCM-41 [9] and SBA-15 [10] in powder or in thin films silica [11] and non-silicate [12] oxide.

In this article, we focus on the use of hyperpolarised xenon NMR spectroscopy to understand the structure of these mesoporous materials.

2. Experimental

2.1. Materials

The synthesis and characterisation of MCM-41 used in this work were described elsewhere [13]. The powders with template were calcined at 773 K in the flow of oxygen.

SBA-15 mesoporous solids were synthesised by using tetraethyl orthosilicate (TEOS), and triblock poly(ethylene oxide)-poly(propylene oxide)-poly(ethylene oxide) (EO_{20} $PO_{70}EO_{20}$) Pluronic P-123 copolymers. The synthesis conditions were described elsewhere [14]. The structural parameters of the samples under study are presented in Table 1.

Arenesulfonic-functionalised mesoporous silica samples were synthesised using the co-condensation of TEOS and 2-(4-chlorosulfonyl) ethyltrimethoxysilane (CSPTMS) in the presence of a poly(alkylene oxide) block copolymer (Pluronic P-123). The molar composition of the studied material was: $(1-x)$ SiO_2: xCSTPMS:6.5 HCl:180 H_2O, where $x = 0.15$.

* Corresponding author.
E-mail address: antoine.gedeon@upmc.fr (A. Gédéon).

0920-5861/$ – see front matter © 2005 Elsevier B.V. All rights reserved.
doi:10.1016/j.cattod.2005.11.069

Table 1
Structural parameters for the studied MCM-41 and SBA-15 samples

Sample	S_{BET} (m^2/g)	Pore diameter (nm)
MCM-41	1065	3.9
SBA-100 °C	993	6.7
SBA-60 °C	938	4.2
SBA-SO_3H	623	6.5

The mesoporous silica thin films having 2D hexagonal, 3D hexagonal and 3D cubic structures were prepared using the sol–gel chemistry process using CTAB as surfactants [15]. The thin films were deposited on a glass substrate using the dip-coating method. While the substrate is withdrawn, evaporation occurs and leads to a self-assembly condensation process.

2.2. Optical pumping setup

The continuous flow system for the production of hyperpolarised xenon based on the design of Ref. [16] was described elsewhere [17]. Circular polarised light from a 60 W diode array laser (COHERENT) was used for optical pumping at the D1 transition of rubidium (794.7 nm) within a Pyrex pumping cell containing a small amount of rubidium vapour and placed in the fringe field of the superconducting magnet. The Xe–He mixtures containing 0.5–1000 Torr of Xe purified using oxygen trap, polarised to ca. 1% at total pressure of 1000 Torr, were circulated at ca. 100 cc/min flow rate through the samples.

2.3. NMR

The spectra were recorded at 7 T using a Bruker AMX300 spectrometer operating at 83.02 MHz for ^{129}Xe. Prior to the NMR measurements, MCM-41 and SBA-15 samples were made into pellets of ca. 0.2 mm thickness by applying pressure at 380 MPa. For flow experiments, the pellets were broken into smaller pieces that fit into a 10 mm o.d. NMR tube equipped with two Young valves. The samples were subsequently evacuated at 573 K for 12 h. For the supported films, six slices were cut into 0.3 cm × 1.5 cm pieces, which represent about 0.1 mg of SiO_2 or TiO_2 and placed into the NMR tube. 8–1024 FIDs were acquired using 10 μs ($\pi/2$) pulses and 1–30 s relaxation delays. The signal of xenon gas at 10 Torr is used as the reference of the chemical shifts.

3. Results and discussions

3.1. ^{129}Xe chemical shift

Based on the fast exchange concept [2], and in the absence of strong adsorption sites, the chemical shift δ_i of xenon adsorbed on site i can be presented as the sum of the terms corresponding to the different perturbations to which xenon is subjected: $\delta_i = \delta_0 + \delta_s + \delta_{Xe}$, where δ_0 is the chemical shift of xenon gas at zero pressure and δ_s is the contribution due to xenon interacting with the surface of the solid. This term can reflect the geometry of the xenon environment on the surface. The contribution δ_{Xe} is due to xenon–xenon collisions. This term is proportional to xenon density, and thus will increase (lower field) when xenon concentration increases.

In the presence of strong adsorption sites (SAS), there will be another contribution to the observed chemical shift. At very low xenon concentration, each xenon spends a relatively long time on the SAS, which would increase the observed chemical shift. At higher xenon concentration the relative population of xenon adsorbed on the SAS decreases and the chemical shift will decrease to the values characteristic of the rest of the surface.

3.2. Variable pressure experiments for MCM-41 and SBA-15 samples

The ^{129}Xe NMR spectra (not shown) of xenon adsorbed on MCM-41 and SBA-15 mesoporous solids at 298 K exhibit the line at 0 ppm peculiar to the xenon in the gas phase and the lines shifted to lower field due to the xenon adsorbed in the pores. Fig. 1 shows the variation of the observed chemical shift against the partial pressure of adsorbed xenon on MCM-41 and two samples of SBA-15 synthesised at 60 and 100 °C, respectively. Chemical shifts of xenon in mesoporous materials depend on their pore size. The bigger the pore diameter, the smaller are the observed shifts [14].

For MCM-41, the ^{129}Xe chemical shift is almost pressure independent, which agrees well with previous results [18–20].

For the SBA-15 sample synthesised at 100 °C, the chemical shift occurs to higher fields when xenon pressures increase, which is typical of the presence of a small amount of SAS in the pores. The most likely candidates for such sites are the micropores in the walls of SBA-15, which presence is well established [21]. The length of such micropores should be of the order of the wall thickness, which for SBA-15 does not exceed several nm, so xenon will be in fast exchange between micro- and mesopores. Similar behaviour of the xenon adsorbed on mesoporous silica has been observed [7b,22]. The tangent of the ^{129}Xe chemical shift provides further information on the micropore size. The increase of the chemical shift when pressure increases for SBA-15 synthesised at 60 °C indicates that each micropore is large enough to accommodate more than one Xe atom. This suggests that the micropores in this sample are larger than twice the kinetic diameter of xenon (d_{Xe} = 3.96 Å) along at least one direction.

Such a size would be in fair agreement with the genesis of the micropores, formed by the polymerisation of silica around loops of the poly(oxyethylene) chains, normally protruding up to 9 Å from the surface of a micelle of nonionic surfactant [23].

3.3. Arenesulfonic-functionalised SBA-15 material

Fig. 2 displays HP-^{129}Xe NMR spectra of an arenesulfonic SBA-15 sample after calcinations treatment, measured at different pressures. Fig. 3 shows ^{129}Xe chemical shift at different pressures. Unlike purely siliceous SBA-15 samples, whose ^{129}Xe NMR spectra of the adsorbed Xe exhibited a

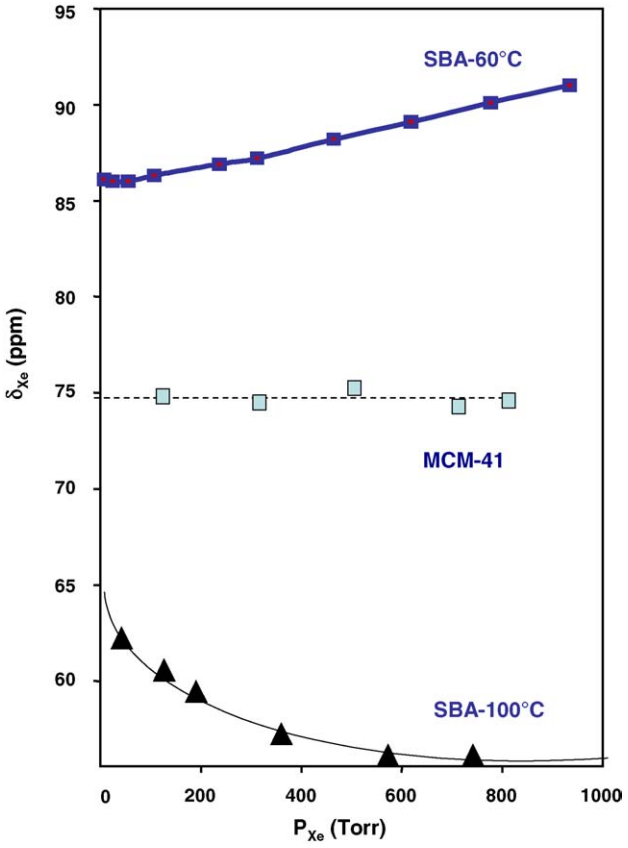

Fig. 1. Variation of ^{129}Xe NMR chemical shift at 298 K vs. xenon pressure for MCM-41 and SBA-15 synthesised at 60 and 100 °C, respectively.

symmetrical narrow peak, broader and somewhat asymmetric lines were observed for the functionalised sample.

Two overlapped peaks at 109 ppm (peak A) and 116 ppm (peak B) were observed at 20 Torr. These peaks are partially resolved at high pressure. This observation demonstrates that in the sample Xe is in fast exchange between two distinct adsorption regions. Thus, we attribute the shoulder at 109 ppm (peak A) to the xenon adsorbed in the bare mesopore silica and the peak B to the xenon interacting with the surface-bound organic phase. The variation of the xenon chemical shift of peaks A and B is shown in Fig. 3. The decrease of δ(B) when the pressure decreases proves the presence of strong adsorption sites, e.g. shallow micropores at the surface of the SBA walls (''rugosity'') that can only accept a single xenon atom.

However, the fact that δ(A) is pressure independent, proves that the probed surface has no defects and all the micropores are occupied by an arenesulfonic group.

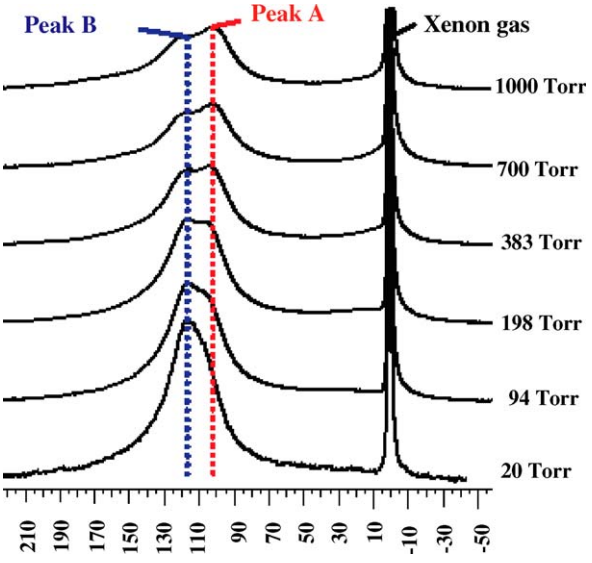

Fig. 2. Evolution of peaks A and B with the HP xenon pressure.

3.4. Mesoporous silica films

Fig. 4 shows the ^{129}Xe NMR spectrum of the HP xenon adsorbed on the supported mesoporous silica films at 163 K. The intense line at 0 ppm in this spectrum is related to xenon in the gas phase.

The other signal corresponds to the xenon adsorbed on the surface of the film pores. The measured chemical shift reflects the structure of the film. Unlike conventional ^{129}Xe NMR techniques, HP ^{129}Xe is a very sensitive detection of xenon local structures.

3.5. Temperature-dependence of ^{129}Xe NMR spectra for MCM-41 and SBA-15 samples

Dynamics of adsorbed xenon in confined geometry and subsequently the morphology of the porous surface can be studied by measuring ^{129}Xe NMR spectra as a function of temperature. The temperature-dependence of the chemical shifts may provide information on the enthalpy of xenon adsorption and homogeneity of the pore surface.

The temperature dependencies of the chemical shift of xenon adsorbed on the studied samples are summarised in Fig. 5. An interesting feature of low-temperature measurements in these samples is the fact that the spectra of thermally polarised (TP) xenon become easily detectable (within several minutes of accumulation without laser irradiation) at temperatures below 253 K due to a higher adsorption of xenon.

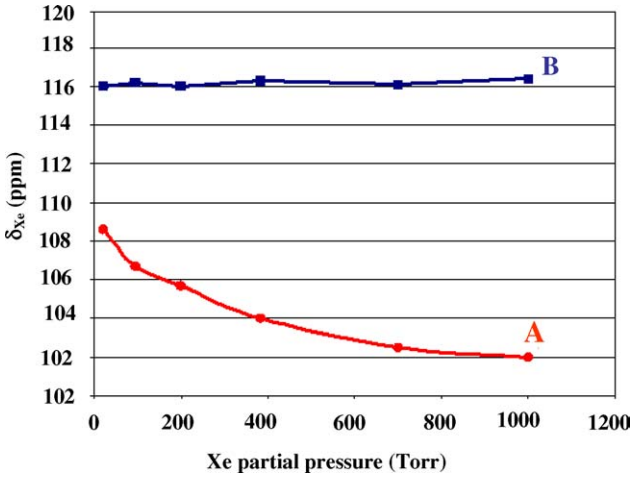

Fig. 3. Variation of ^{129}Xe NMR chemical shift at 298 K vs. xenon pressure for SBA-SO_3H sample.

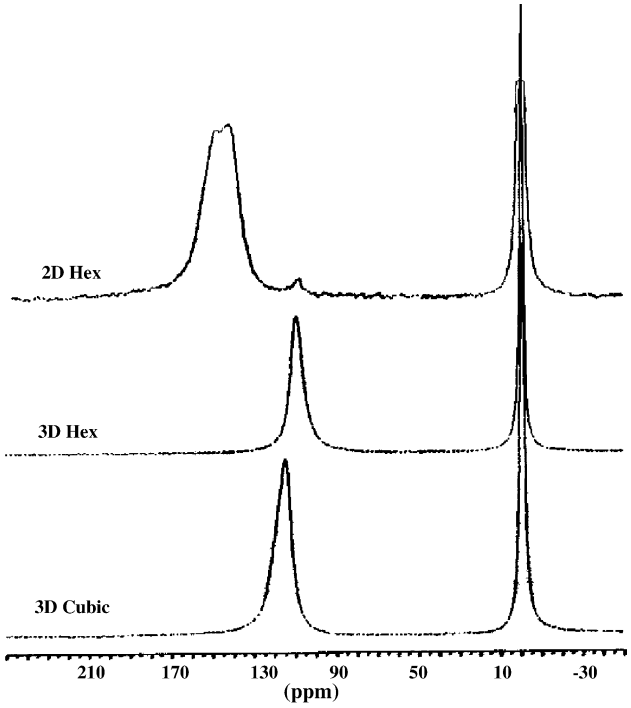

Fig. 4. The HP ^{129}Xe spectrum, acquired at 163 K, of the xenon adsorbed on silica films with different hexagonal (Hex) or cubic structures.

Chemical shifts of TP xenon coincide within the experimental error with those of HP xenon, which indicates that, in our case, the spectra truly represent the properties of the entire sample, despite the fact that HP xenon does not probe all its volume.

For the supported silica film, the signals observed at room and just below room temperature and just below are very different from those observed in the case of mesoporous powders [8], which are usually much narrower. The reasons for such broad signals at room temperature can be a distribution of pore diameters, a poor organisation of the mesoporous phase and/or the exchange process between xenon adsorbed in the pores and on the outer surface of the film. The former two explanations can be ruled out since TEM and XRD data show a quite narrow distribution of pore sizes and a high degree of order of the mesoporous structure [8].

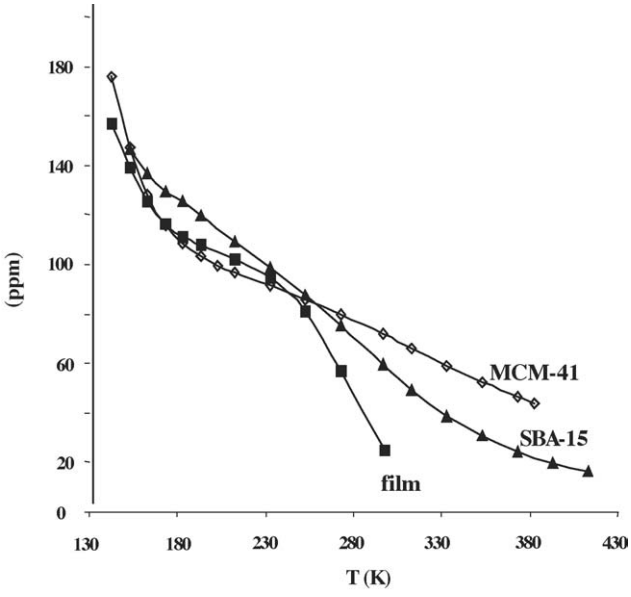

Fig. 5. Effect of temperature on the chemical shift of the xenon adsorbed on MCM-41, SBA-15 (100 °C) and silica thin film (2D hexagonal).

The exchange phenomena are known to be responsible for broadening of NMR signals of Xe in mesoporous powders in the case of small particle dimensions (<10 μm) due to the formation of an interparticle secondary pore system. In our case, such a severe broadening is impossible, since this mesoporous continuous film is free of interparticle pores. The observed broadening could thus be attributed to the presence of shallow mesopores, in which xenon atoms are not confined, but spend most of time in the outer space. When temperature decreases, exchange with the gas phase drastically slows down and the observed chemical shift becomes function of the chemical composition of the surface and of the Xe–Xe interactions in the adsorbed layer. The comparison of the evolutions of the xenon chemical shift values with temperature in MCM-41, SBA-15 powders and in film (Fig. 3) illustrates these ideas.

To obtain quantitative information on xenon adsorption, let us consider the expression of the observed chemical shift δ_{obs}. Under the conditions of fast exchange, δ_{obs} can be expressed as $\delta_{obs} = \sum \delta_i N_i$, where δ_i is the chemical shift of xenon adsorbed on site i and N_i is the relative xenon population on site i.

Taking the chemical shift of xenon in the gas phase $\delta_0 = 0$, and assuming that xenon adsorbed in the pores is described by Henry's law, one can obtain:

$$\delta = \frac{\delta_a}{1 + \frac{D}{f k_{ads} RT}} \tag{1}$$

where δ_a is the chemical shift of adsorbed xenon on the surface, D the pore diameter, k_{ads} the Henry constant at temperature T, R the ideal gas constant and f a pore geometry factor.

The Henry constant, which is temperature dependent, can be expressed as

$$k_{ads}(T) = \frac{k_0}{\sqrt{T}} \exp\left(-\frac{Q_{ads}}{RT}\right) \tag{2}$$

where Q_{ads} is the effective heat of adsorption for the pores under consideration and k_0 is the pre-exponent factor which does not depend on temperature.

Combining Eqs. (1) and (2), the observed chemical shift can be expressed as

$$\delta = \frac{\delta_a}{1 + \left(D / f k_0 R T^{1/2} \exp\left(-\frac{Q_{ads}}{RT}\right)\right)} \tag{3}$$

In logarithmic coordinates, Eq. (3) transforms to:

$$\ln\left(\frac{1}{\delta} - \frac{1}{\delta_a}\right) + \frac{1}{2} \ln T = \ln \frac{D}{\delta_a f k_0 R} + \frac{Q_{ads}}{RT} \tag{4}$$

In the high temperature region, where the adsorption of xenon and hence, xenon–xenon interactions in the adsorbed layer are low, and for the case where D and δ_a do not depend on temperature, it is possible to determine the heats of xenon adsorption by plotting $[\ln(1/\delta - 1/\delta_a) + 0.5 \ln T]$ versus $1/T$. The values of heats of adsorption (-11.53, -17.3 and 9.1 kJ, for MCM-41, SBA-100 °C and SBA-60 °C, respectively) indicate that, in all cases, physical adsorption takes place.

4. Conclusion

This paper clearly shows that the porosity of silica thin films can be probed directly by using HP ^{129}Xe NMR. The evolution of the ^{129}Xe NMR chemical shift with pressure allows to detect the presence of microporosity in SBA-15 materials. Variable temperature measurements allowed us to evaluate the heats of adsorption of xenon adsorbed on different types of mesoporous solids.

References

[1] (a) T. Ito, J. Fraissard, J. Chem. Phys. 76 (1982) 5225;
(b) J. Ripmeester, J. Am. Chem. Soc. 104 (1982) 289.
[2] (a) D. Raftery, B. Chmelka, Nucl. Magn. Reson. Basic Princ. Prog. 30 (1994) 111;
(b) J.L. Bonardet, J. Fraissard, A. Gédéon, M.A. Springuel-Huet, Catal. Rev. 41 (1999) 117.
[3] T. Pietrass, J.M. Kneller, R.A. Assink, M.T. Anderson, J. Phys. Chem. B 103 (1999) 8837.
[4] (a) B.C. Grover, Phys. Rev. Lett. 40 (1978) 391;
(b) W. Happer, E. Miron, S. Shaefer, Van Wingaarden, X. Zeng, Phys. Rev. A 29 (1984) 3092.
[5] D. Raftery, E. Mac Namara, G. Fisher, C.V. Rice, J. Smith, J. Am. Chem. Soc. 119 (1997) 8746.
[6] (a) M. Haake, A. Pines, J. Reiner, R. Seydoux, J. Am. Chem. Soc. 119 (1997) 11711;
(b) R. Seydoux, A. Pines, M. Haake, J. Reimer, J. Phys. Chem. B 103 (1999) 4629.
[7] (a) I. Moudrakovski, V. Terskikh, C. Ratcliffe, J. Ripmeester, L.Q. Wang, Y. Shin, G. Exarhos, J. Phys. Chem. B 106 (2002) 5938;
(b) A. Nossov, E. Haddad, F. Guenneau, A. Gédéon, Phys. Chem. Chem. Phys. 5 (2003) 4473.
[8] (a) A. Nossov, E. Haddad, F. Guenneau, C. Mignon, A. Gédéon, D. Grosse, C. Bonhomme, F. Babonneau, C. Sanchez, Chem. Commun. 21 (2002) 2476;
(b) D. Grosso, F. Cagnol, G.J. de A.A. Soler-Illia, A. Bourjois, A. Brunet-Bruneau, C. Sanchez, Adv. Funct. Mater. 14 (2004) 309.
[9] C.T. Kresge, M.E. Leonowicz, W.J. Roth, J.C. Vartuli, J.S. Beck, Nature 359 (1992) 710;
(b) C.J. Brinker, Y. Lu, A. Sellinger, H. Fan, Adv. Mater. 11 (1999) 579.
[10] D. Zhao, P. Yang, N. Melosh, J. Feng, B.F. Chmelka, G.D. Stucky, Adv. Mater. 10 (1998) 1380.
[11] D. Grosso, G.J. de A.A. Soler-Illia, F. Babonneau, C. Sanchez, P.A. Albouy, A. Brunet-Bruneau, A.R. Balkenende, Adv. Mater. 13 (2001) 1085.
[12] D. Grosso, F. Babonneau, P.A. Albouy, H. Amenitsch, A.R. Balkenende, A. Brunet-Bruneau, J. Rivory, Chem. Mater. 14 (2002) 931.
[13] V. Fenelonov, V. Romannikov, A. Derevyankin, Microporous Mesoporous Mater. 28 (1999) 57.
[14] A. Galarneau, J. Cambon, T. Martin, L.C. de Menorval, D. Brunel, F. Di Renzo, Fajula, Stud. Surf. Sci. Catal. 142 (2002) 395.
[15] E.L. Crepaldi, G.J. Soler-Ille, D. Grosso, C. Sanchez, New J. Chem. 27 (2003) 9.
[16] (a) B.C. Grover, Phys. Rev. Lett. 40 (1978) 391;
(b) W. Happer, E. Miron, S. Shaefer, Van Wingaarden, X. Zeng, Phys. Rev. A 29 (1984) 3092.
[17] (a) D. Raftery, H. Long, T. Meersmann, P.J. Grandinetti, L. Reven, A. Pines, Phys. Rev. Lett. 66 (1991) 584;
(b) A. Nossov, F. Guenneau, M.-A. Springuel-Huet, E. Haddad, V. Montouillout, B. Knott, F. Engelke, C. Fernandez, A. Gedeon, Phys. Chem. Chem. Phys. 5 (2003) 4479.
[18] F. Cros, J.-P. Korb, L. Malier, Langmuir 16 (2000) 10193.
[19] C.J. Jameson, A.K. Jameson, H.-M. Lim, B.I. Baello, J. Chem. Phys. 100 (1996) 5977.
[20] E. Haddad, J.-B. d'Espinose, A. Nossov, F. Guenneau, A. Gédéon, Stud. Surf. Sci. Catal. 142 (2002) 1173.
[21] A. Galarneau, H. Cambon, F. Di Renzo, R. Ryoo, M. Choi, F. Fajula, New J. Chem. 27 (2003) 73.
[22] I. Moudrakovski, V. Terskikh, C. Ratkliffe, J. Ripmeester, J. Phys. Chem. B 106 (2002) 5938.
[23] J.N. Israelchvili, H. Wennerström, J. Phys. Chem. 96 (1992) 520.